

# Practical Quantum Computing: solving the wave equation using a quantum approach

Adrien Suau,<sup>1, 2,\*</sup> Gabriel Staffelbach,<sup>1</sup> and Henri Calandra<sup>3</sup>

<sup>1</sup>*CERFACS, 42 Avenue G. Coriolis, 31057 Toulouse, France*

<sup>2</sup>*LIRMM, Univ Montpellier, CNRS, Montpellier, France*

<sup>3</sup>*TOTAL SA, 2 Avenue Vignancour, 64000 Pau, France*

(Dated: May 10, 2022)

In the last years, several quantum algorithms that try to address the problem of partial differential equation solving have been devised. On one side, the “direct” quantum algorithms that aim at encoding the solution of the PDE by executing one large quantum circuit. On the other side, variational algorithms that approximate the solution of the PDE by executing several small quantum circuits and making profit of classical optimisers. In this work we propose an experimental study of the costs (in terms of gate number and execution time on a idealised hardware created from realistic gate data) associated with one of the “direct” quantum algorithm: the wave equation solver devised in [PCS. Costa, S. Jordan, A. Ostrander, *Phys. Rev. A* 99, 012323, 2019]. We show that our implementation of the quantum wave equation solver agrees with the theoretical big-O complexity of the algorithm. We also explain in great details the implementation steps and discuss some possibilities of improvements. Finally, our implementation proves experimentally that some PDE can be solved on a quantum computer, even if the direct quantum algorithm chosen will require error-corrected quantum chips, which are not believed to be available in the short-term.

## I. INTRODUCTION

Quantum computing has drawn a lot of attention in the last few years, following the successive announcements from several world-wide companies about the implementation of quantum hardware with an increasing number of qubits or reduced error rates [1–5].

Along with the hardware improvement, new quantum algorithms were discovered, yielding potential quantum speed-up and applications in various fields such as quantum chemistry [6], linear algebra [7–12] or optimisation [13–15]. Recent works even show that differential equations may be solved by using a quantum computer [16–27]. But despite the large number of algorithms available, it is hard to find an actual implementation of a quantum differential equation solver, Hamiltonian simulation being the unique exception by solving the time-dependant Schrödinger equation.

In this work, we present and analyse a quantum wave equation solver we implemented from scratch according to the algorithm depicted in [28]. During the solver implementation, we had to look for a Hamiltonian Simulation procedure. The implementations we found being too restricted, we decided to implement our own Hamiltonian Simulation procedure, which will also be analysed.

To the best of our knowledge, this work is the first to analyse experimentally the characteristics of a quantum PDE solver. We checked that the practical implementation agrees with the theoretical asymptotic complexities on several quantities of interest such as the total gate count with respect to the number of discretisation points used or the precision, the number of qubits required versus the number of discretisation points used

to approximate the solution or precision of the solution when compared to a classical finite-difference solver. Finally, we verified that the execution time of the generated quantum circuit on today’s accessible quantum hardware was still following the theoretical asymptotic complexities devised for the total gate count. Quantum hardware data were extracted from IBM Q chips.

We show experimentally that it is possible to solve the 1-dimensional wave equation on a quantum computer with a time-complexity that grows as  $\mathcal{O}\left(N_d^{3/2} \log(N_d)^2\right)$  where  $N_d$  is the number of discretisation points used to approximate the solution. But even if the asymptotic scaling is better than classical algorithms, we found out that the constants hidden in the big-O notation were huge enough to make the solver less performant than classical solvers for reasonable discretisation sizes.

## II. PROBLEM CONSIDERED

We consider a simplified version of the wave equation on the 1-dimensional line  $[0, 1]$  where the propagation speed  $c$  is constant and equal to 1. This equation can be written as

$$\frac{\partial^2}{\partial t^2} \phi(x, t) = \frac{\partial^2}{\partial x^2} \phi(x, t). \quad (1)$$

Moreover, we only consider solving Equation (1) with the Dirichlet boundary conditions

$$\frac{\partial}{\partial x} \phi(0, t) = \frac{\partial}{\partial x} \phi(1, t) = 0. \quad (2)$$

No assumption is made on initial speed  $\phi(x, 0)$  and initial velocity  $\frac{\partial \phi}{\partial t}(x, 0)$ .

\* adrien.suau@cerfacs.fr

The resolution of this simplified wave equation on a quantum computer is an appealing problem for the first implementation of a PDE solver for several reasons. First, the wave equation is a well-known and intensively studied problem for which a lot of theoretical results have been verified. Secondly, even-though it is a relatively simple PDE, the wave equation can be used to solve some interesting problems such as seismic imaging [29, 30]. Finally, the theoretical implementation of a quantum wave equation solver has already been studied in [31].

In this paper, we present the complete implementation of a 1-dimensional wave equation solver using quantum technologies based on `qat` library. To the best of our knowledge, this work is the first to consider the implementation of an entire PDE solver that can run on a quantum computer. Specifically, we explain all the implementation details of the solver from the mathematical theory to the actual quantum circuit used. The characteristics of the solver are then discussed and analysed, such as the estimated gate count and estimated execution time on real quantum hardware. We show that the implementation follows the theoretical asymptotic behaviours devised in [28]. Moreover, the wave equation solver algorithm relies critically on an efficient implementation of a Hamiltonian simulation algorithm, which we have also implemented and analysed thoroughly.

### III. IMPLEMENTATION

The algorithm used to solve the wave equation is explained in [28] and uses a Hamiltonian simulation procedure. Costa *et al.* chose the Hamiltonian simulation algorithm described in [32] for its nearly optimal theoretical asymptotic behaviour. We privileged instead the Hamiltonian simulation procedure explained in [33, 34] for its good experimental results based on [31] and its simpler implementation (detailed in Appendix A).

The code has been written using `qat`, a Python library shipped with the Quantum Learning Machine (QLM), a package developed and maintained by Atos. It has not been extensively optimized yet, which means that there is still a large room for improvements. Possible optimizations and improvements are discussed in Appendix E.

All the circuits used in this paper have been generated with a subset of `qat`'s gate set:

$$\{H, X, R_y(\theta), P_h(\theta), CP_h(\theta), CNOT, CCNOT\} \quad (3)$$

and have then been translated to the gate set

$$\{U_1(\lambda), U_2(\lambda, \phi), U_3(\lambda, \phi, \theta), CNOT\} \quad (4)$$

for  $U_1$ ,  $U_2$  and  $U_3$  defined in Equation (7) of [35] as follow:

$$U(\lambda, \phi, \theta) = \begin{pmatrix} \cos\left(\frac{\theta}{2}\right) & -e^{i\lambda} \sin\left(\frac{\theta}{2}\right) \\ e^{i\phi} \sin\left(\frac{\theta}{2}\right) & e^{i(\lambda+\phi)} \cos\left(\frac{\theta}{2}\right) \end{pmatrix} \quad (5)$$

$$U_3(\lambda, \phi, \theta) = U(\lambda, \phi, \theta) \quad (6)$$

$$U_2(\lambda, \phi) = U\left(\frac{\pi}{2}, \lambda, \phi\right) \quad (7)$$

$$U_1(\lambda) = U(0, 0, \lambda) \quad (8)$$

**Note 1.** The target gate set presented in Equation (4) does not correspond to the physical gate set implemented by IBM hardware (see Equation (8) of [35]). This choice is justified by the fact that IBM only provides hardware characteristics such as gate times for the gate set of Equation (4) and not for the real hardware gate set.

**Note 2.** Our implementation ignores several practical details such as hardware topology or the number of available qubits.

This implementation aims at validating in practice the theoretical asymptotic complexities of Hamiltonian simulation algorithms and providing a proof-of-concept showing that it is possible to solve a partial differential equation on a quantum computer.

#### A. Sparse Hamiltonian simulation algorithm

**Definition 1. *s*-sparse matrix:** A  $s$ -sparse matrix with  $s \in \mathbb{N}^*$  is a matrix that has at most  $s$  non-zero entries per row and per column

**Definition 2. *s*-sparse matrix:** A sparse matrix is a  $s$ -sparse matrix with  $s \in \mathcal{O}(\log(N))$ ,  $N$  being the size of the matrix.

In the past years, a lot of algorithms have been devised to simulate the effect of a Hamiltonian on a quantum state [32, 34, 36–45]. Among all these algorithms, only few have already been implemented for specific cases [46, 47] but to the best of our knowledge no implementation is currently capable of simulating a generic sparse Hamiltonian.

The domain of application of the already existing methods being too narrow, we decided to implement our own generic sparse Hamiltonian simulation procedure. We based our work on the product-formula approach described in [33, 34]. One advantage of this approach is that product-formula based algorithms have already been thoroughly analysed both theoretically [33, 34] and practically [31, 48], and several implementations are publicly available, though restricted to Hamiltonians that can be decomposed as a sum of tensor products of Pauli matrices. Moreover, [33] provides a lot of implementation details that allowed us to go straight to the development step.

Our implementation is capable of simulating an arbitrary sparse Hamiltonian provided that it has already been decomposed into a sum of 1-sparse Hermitian matrices with either only real or only complex entries, each described by an oracle. The implementation has been validated with several automated tests and a more complex case involving the simulation of a 2-sparse Hamiltonian and described in Section III B. Furthermore, it

agrees perfectly with the theoretical complexities devised in [33, 34] as studied and verified in Section IV.

### B. Quantum wave equation solver

Using the Hamiltonian simulation algorithm implementation, we successfully implemented a 1-dimensional wave equation solver using the algorithm described in [28] and explained in appendices B and C.

For the specific case considered (Eq. (1) and (2)), solving the wave equation for a time  $T$  on a quantum computer boils down to simulating a 2-sparse Hamiltonian for a time  $f(T)$ , the function  $f$  being thoroughly described in [28] and Equation (18). The constructed quantum circuit can then be applied to a quantum state representing the initial position  $\psi(x, 0)$  and velocity  $\frac{\partial\phi}{\partial t}(x, 0)$ , and will evolve this state towards a quantum state representing the final position  $\phi(x, T)$  and velocity  $\frac{\partial\phi}{\partial t}(x, T)$ .

As for the Hamiltonian simulation procedure, the practical results we obtain from the implementation of the quantum wave equation solver seems to match the theoretical asymptotic complexities. See Section IV for an analysis of the theoretical asymptotic complexities.

## IV. RESULTS

Using a simulator instead of a real quantum computer has several advantages. In terms of development process, a simulator allows the developer to perform several actions that are not possible as-is on a quantum processor such as describing a quantum gate with a unitary matrix instead of a sequence of hardware operations. Another useful operation that is possible on a quantum simulator and not currently achievable on a quantum processor is efficient generic state preparation.

Our implementation uses only standard quantum gates and does not leverage any of the simulator-only features such as quantum gates implemented from a unitary matrix. In other words, both the Hamiltonian simulation procedure and the quantum wave equation solver are “fully quantum” and are readily executable on a quantum processor, provided that it has enough qubits. As a proof, and in order to benchmark our implementation, we translated the generated quantum circuits to IBM Q Melbourne gate-set (see Equation (4)). IBM Q Melbourne [49] is a quantum chip with 14 usable qubits made available by IBM the 23<sup>th</sup> of September, 2018.

**Note 3.** We chose IBM Q Melbourne mainly because, at the time of writing, it was the publicly accessible quantum chip with the larger number of qubits and so was deemed to be the closest to future quantum hardware. It is important to note that even if IBM Q Melbourne has 14 qubits, the quantum circuits constructed in this paper are not runnable because they require more qubits. Consequently, because of this hardware limitation, hardware topology has also been left apart of the study.

This allowed us to have an estimation of the number of hardware gates needed to either solve the wave equation or simulate a specific Hamiltonian on this specific hardware. Combining these numbers and the hardware gate execution time published in [50], we were able to compute a rough approximation of the time needed to solve the considered problem presented in Equations (1) and (2) on this specific hardware.

### A. Hamiltonian simulation

As explained in Section III A, the Hamiltonian simulation algorithm implemented has been first devised in [33, 34]. A quick review of the algorithm along with implementation details can be found in Appendix A. This Hamiltonian simulation procedure requires that the Hamiltonian matrix  $H$  to simulate can be decomposed as

$$H = \sum_{j=1}^m H_j \quad (9)$$

where each  $H_j$  is an efficiently simulable Hermitian matrix.

In our benchmark, we simulated the Hamiltonian described in Equation (B11). According to [33], real 1-sparse Hermitian matrices with only 1 or 0 entries can be simulated with  $\mathcal{O}(n)$  gates and 2 calls to the oracle,  $n$  being the number of qubits the Hamiltonian  $H$  acts on.

Let  $O_i$  be the gate complexity of the oracle implementing the  $i^{\text{th}}$  Hermitian matrix  $H_i$  of the decomposition (9), we end up with an asymptotic complexity of  $\mathcal{O}(n + O_i)$  to simulate  $H_i$ .

Applying the Trotter-Suzuki product-formula of order  $k$  (see Definition 4 in Appendix A 5 for the definition of the Trotter-Suzuki product-formula) on the quantum circuit simulating the Hermitian matrices produces a circuit of size

$$\mathcal{O}\left(5^k \sum_{i=1}^m (n + O_i)\right). \quad (10)$$

This circuit should finally be repeated  $r$  times in order to achieve an error of at most  $\epsilon$ , with

$$r \in \mathcal{O}\left(5^k m \tau \left(\frac{m \tau}{\epsilon}\right)^{\frac{1}{2k}}\right), \quad (11)$$

and  $\tau = t \max_i \|H_i\|$ ,  $t$  being the time for which we want to simulate the given Hamiltonian and  $\|\cdot\|$  being the spectral norm [34].

Merging Equations (10) and (11) gives us the complexity

$$\mathcal{O}\left(5^{2k} m \tau \left(\frac{m \tau}{\epsilon}\right)^{\frac{1}{2k}} \sum_{i=1}^m (n + O_i)\right). \quad (12)$$

This generic expression of the asymptotic complexity can be specialized to our benchmark case. The number of gates needed to implement the oracles is  $\mathcal{O}(n^2)$  and the chosen decomposition contains  $m = 2$  Hermitian matrices, each with a spectral norm of 1. Replacing the symbols in Equations (10) and (11) results in the asymptotic gate complexity of

$$\mathcal{O}(5^{2k}n^2) \quad (13)$$

for the circuit simulating  $e^{-iHt/r}$  and a number

$$r \in \mathcal{O}\left(5^k t \left(\frac{t}{\epsilon}\right)^{\frac{1}{2k}}\right) \quad (14)$$

of repetitions, which lead to a total gate complexity of

$$\mathcal{O}\left(5^{2k}n^2 t \left(\frac{t}{\epsilon}\right)^{\frac{1}{2k}}\right). \quad (15)$$

In order to check that our implementation follows this theoretical asymptotic behaviour, we chose to let  $k = 1$  and plotted the number of gates generated versus the three parameters that have an impact on the number of gates: the number of discretisation points  $N_d$  (Figure 1), the time of simulation  $t$  (Figure 2) and the precision  $\epsilon$  (Figure 3). The corresponding asymptotic complexity should be

$$\mathcal{O}\left(n^2 \frac{t^{3/2}}{\sqrt{\epsilon}}\right) = \mathcal{O}\left(\log_2(N_d)^2 \frac{t^{3/2}}{\sqrt{\epsilon}}\right). \quad (16)$$

## B. Wave equation solver

The first characteristic of the wave equation solver that needs to be checked is its validity: is the quantum wave equation solver capable of solving accurately the wave equation as described in Equations (1) and (2)?

To check the validity of the solver, we used `qat` simulators and Atos QLM to simulate the quantum program generated to solve the wave equation with different values for the number of discretisation points  $N_d$ , for the physical time  $t$  and for the precision  $\epsilon$ . Figure 5 shows the classical solution versus the quantum solution and the absolute error between the two solutions for  $N_d = 32$ ,  $t = 0.4$  and  $\epsilon = 10^{-3}$ . The solution obtained by the quantum solver is nearly exactly the same as the classical solution obtained with finite differences. The error between the two solutions is of the order of  $10^{-7}$ , which is 4 orders of magnitudes smaller than the error we asked for.

Once the validity of our solver has been checked on multiple test cases, the next interesting property we would like to verify is the asymptotic cost: does the implemented simulator seems to agree with the theoretical asymptotic complexities derived from [28] and [34]?

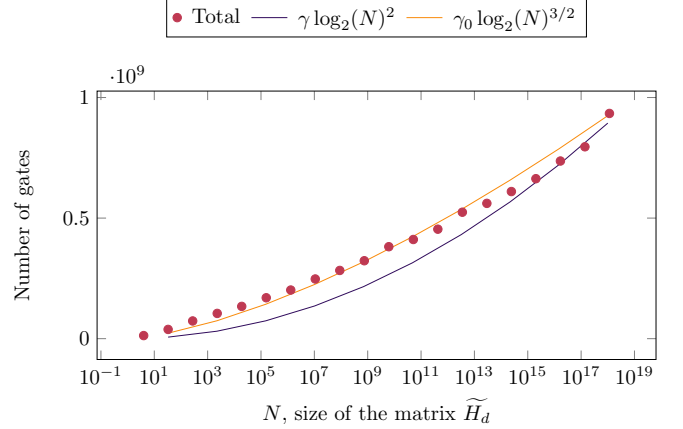


Figure 1. Plot of the number of quantum gates needed to simulate the Hamiltonian described in Appendix B using the oracles implemented following Appendix C. Graph generated with a Trotter-Suzuki product-formula order  $k = 1$ , a physical time  $t = 1$  and a precision  $\epsilon = 10^{-5}$ . The value of the constant  $\gamma = 210000$  has been chosen arbitrarily to fit the experimental data. A small discrepancy can be observed: the data seems to be better fitted by  $\log_2(N)^{3/2}$  instead of the theoretical  $\log_2(N)^2$ . This non-concordance may be due to the fact that the quantity observed (number of gates) has not reached its asymptotic behaviour yet.

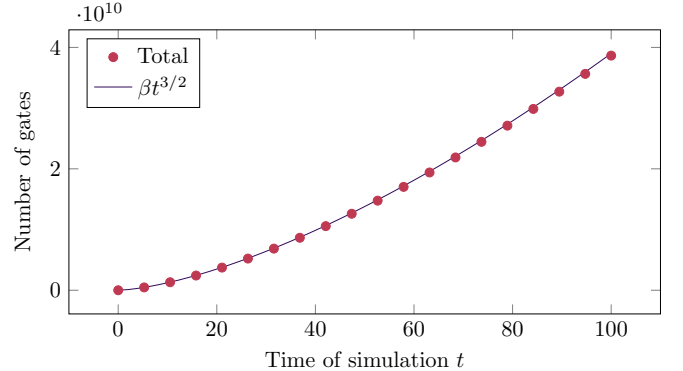


Figure 2. Plot of the number of quantum gates needed to simulate the Hamiltonian described in Appendix B using the oracles implemented following Appendix C. Graph generated with a Trotter-Suzuki product-formula order  $k = 1$ , 32 discretisation points (i.e.  $n = 6$  qubits) and a precision  $\epsilon = 10^{-5}$ . The value of  $\beta = 39000000$  has been chosen arbitrarily to fit the experimental data.

In our specific case, the Hamiltonian  $H$  to simulate can be decomposed in two 1-sparse Hermitian matrices, both of them having a spectral norm of 1. The exact decomposition can be found in Section B3. We chose to let the product-formula order be equal to  $k = 1$  and reuse the asymptotic complexity found in Equation (15) by changing the time of simulation  $t$  by the time  $f(t)$ :

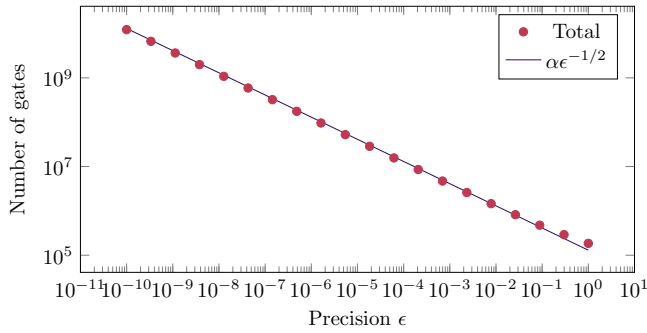


Figure 3. Plot of the number of quantum gates needed to simulate the Hamiltonian described in Appendix B using the oracles implemented following Appendix C. Graph generated with a Trotter-Suzuki product-formula order  $k = 1$ , 32 discretisation points (i.e.  $n = 6$  qubits) and a time  $t = 1$ . The value of  $\alpha = 130000$  has been chosen arbitrarily to fit the experimental data.

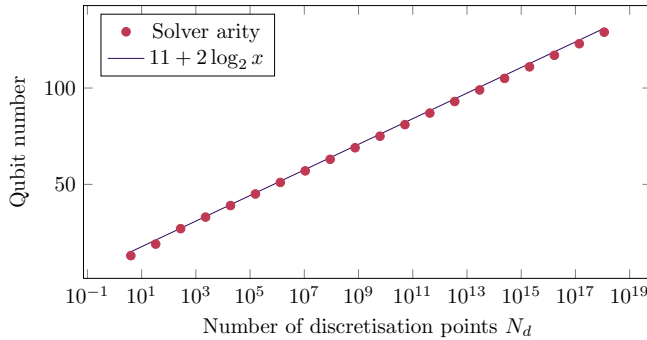


Figure 4. Plot of the number of qubits needed to run the wave equation solver for a time  $t = 1$ , a precision  $\epsilon = 10^{-5}$  and a Trotter-Suzuki product-formula of order  $k = 1$ . The constants values 11 and 2 have been chosen arbitrarily to fit the experimental data.

$$\mathcal{O} \left( 5^{2k} n^2 f(t) \left( \frac{f(t)}{\epsilon} \right)^{\frac{1}{2k}} \right). \quad (17)$$

Following the study performed in [28],

$$f(t) = \frac{t}{\delta x} = t(N_d - 1) \quad (18)$$

where  $\delta x$  is the distance between two discretisation points. Moreover, it is possible to prove (see Appendix B 3) that

$$n = \lceil \log_2(2N_d - 1) \rceil \quad (19)$$

Replacing  $f(t)$  and  $n$  in Equations (10) and (11) gives us a gate complexity of

$$\mathcal{O} (5^k n^2) \quad (20)$$

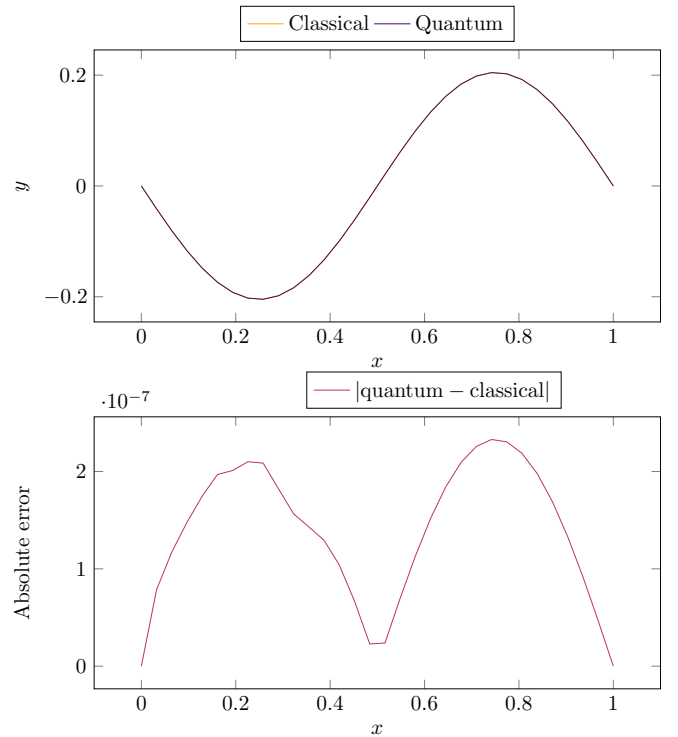


Figure 5. Comparison of the classical solver and the quantum solver. Both solvers solved the 1-D wave equation with  $N_d = 32$  discretisation points and a physical time of  $t = 0.4$ . The classical solver uses finite-differences with a very small time-step in order to avoid as much as possible errors due to time-discretisation. The quantum solver was instructed to solve the wave equation with a precision of at least  $\epsilon = 10^{-3}$ , used a Trotter-Suzuki order of  $k = 1$  with the minimised bound for  $r$ ,  $r_2^{\min}$ , described in [31] and re-introduced in Appendix D. The solutions of the two solvers are too close to be able to notice a difference (they overlap on the graph), that is why a second graph plotting the absolute error between the two solvers is included.

to construct a circuit simulating  $e^{-iHt/r}$  and a number of repetitions

$$r \in \mathcal{O} \left( 5^k t N_d \left( \frac{t N_d}{\epsilon} \right)^{\frac{1}{2k}} \right). \quad (21)$$

Merging the two expression results in a gate complexity of

$$\mathcal{O} \left( 5^{2k} t N_d \log_2(N_d)^2 \left( \frac{t N_d}{\epsilon} \right)^{\frac{1}{2k}} \right). \quad (22)$$

Choosing the Trotter-Suzuki formula order  $k = 1$  gives us a final complexity of

$$\mathcal{O} \left( N_d^{3/2} \log_2(N_d)^2 \frac{t^{3/2}}{\sqrt{\epsilon}} \right) \quad (23)$$

to solve the wave equation presented in Equation (1). This theoretical result is verified experimentally in Figure 7.

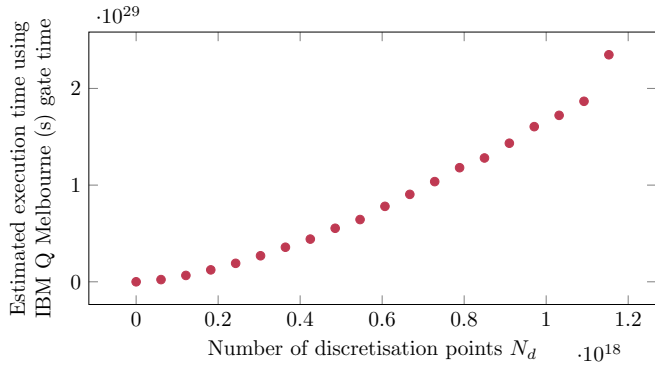


Figure 6. Estimated execution time of the wave equation solver on IBM Q Melbourne hardware. The individual gate times have been extracted from [51] and [50]. The topology of the hardware is not accounted for, which means that we cannot use the GF pulse timings provided in [50]. Instead, we chose to use the arithmetic mean. This graph shows the estimated time with a GF pulse that takes 347ns to complete, GD pulse of 100ns and a buffer time of 20ns.

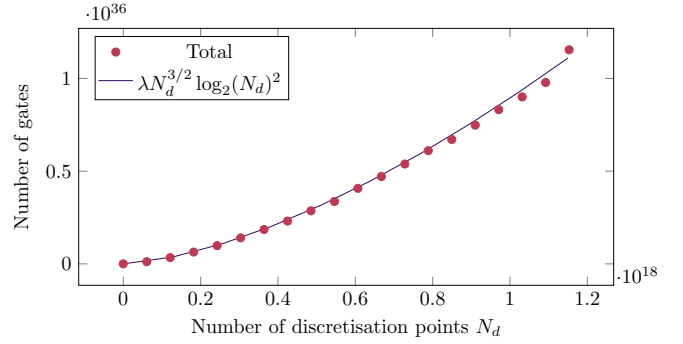


Figure 7. Plot of the number of quantum gates needed to solve the wave equation described in Equation (1). Graph generated with a Trotter-Suzuki product-formula order  $k = 1$ , a physical time  $t = 1$  and a precision  $\epsilon = 10^{-5}$ . The value of  $\lambda = 770000$  has been chosen arbitrarily to fit the experimental data.

**Note 4.** The huge execution time and number of gates presented in Figures 6 and 7 should be interpreted with care as we may be able to reduce them in the future. See Appendix E for an explanation on the possible optimisation.

## V. DISCUSSION

In this work, we focus on the practical cost of implementing a 1-dimensional quantum wave equation solver on a quantum computer. We show that a quantum computer is able to solve partial differential equations by constructing and simulating the quantum circuits described. We also study the scaling of the solver with respect to several parameters of interest and show that the theoretical asymptotic bounds are mostly verified.

In future works, one can study the possibilities of circuit optimisation described in Appendix E. It would also be interesting to implement Neumann boundary conditions instead of Dirichlet ones. A practical implementation including a non-constant propagation speed  $c$  has also been realised during the writing of this paper. The results were encouraging but we decided to not include them in the paper to gain more confidence. Finally, future works might want to extend the wave equation solver to 2 dimensions or more.

## ACKNOWLEDGMENTS

The authors would like to thank Reims University, the ROMEO HPC center, Total, the CCRT and Atos for their support by giving us access to Atos quantum simulator.

---

[1] “Ibm quantum computing,” <https://www.ibm.com/quantum-computing/> (2019), accessed: 2020-03-27.

[2] “Quantum computing — intel newsroom,” <https://newsroom.intel.com/press-kits/quantum-computing/> (2019), accessed: 2020-03-27.

[3] “Quantum supremacy using a programmable superconducting processor,” <https://ai.googleblog.com/2019/10/quantum-supremacy-using-programmable.html> (2019), accessed: 2020-03-27.

[4] F. Arute, K. Arya, R. Babbush, D. Bacon, J. C. Bardin, R. Barends, R. Biswas, S. Boixo, F. G. S. L. Brandao, D. A. Buell, B. Burkett, Y. Chen, Z. Chen, B. Chiaro, R. Collins, W. Courtney, A. Dunsworth, E. Farhi, B. Foxen, A. Fowler, C. Gidney, M. Giustina, R. Graff, K. Guerin, S. Habegger, M. P. Harrigan, M. J. Hartmann, A. Ho, M. Hoffmann, T. Huang, T. S. Humble, S. V. Isakov, E. Jeffrey, Z. Jiang, D. Kafri, K. Kechedzhi, J. Kelly, P. V. Klimov, S. Knysh, A. Korotkov, F. Kostritsa, D. Landhuis, M. Lindmark, E. Lucero, D. Lyakh, S. Mandrà, J. R. McClean, M. McEwen, A. Megrant, X. Mi, K. Michielsen, M. Mohseni, J. Mutus, O. Naaman, M. Neeley, C. Neill, M. Y. Niu, E. Ostby, A. Petukhov, J. C. Platt, C. Quintana, E. G. Rieffel, P. Roushan, N. C. Rubin, D. Sank, K. J. Satzinger, V. Smelyanskiy, K. J. Sung, M. D. Tervitthick, A. Vainsencher, B. Villalonga, T. White, Z. J. Yao, P. Yeh, A. Zalcman, H. Neven, and J. M. Martinis, *Nature* **574**, 505 (2019).

[5] J. M. Pino, J. M. Dreiling, C. Figgatt, J. P. Gaebler, S. A. Moses, C. H. Baldwin, M. Foss-Feig, D. Hayes, K. Mayer, C. Ryan-Anderson, and B. Neyenhuis, (2020), 2003.01293v1.

[6] Y. Cao, J. Romero, J. P. Olson, M. Degroote, P. D. Johnson, M. Kieferová, I. D. Kivlichan, T. Menke, B. Peropadre, N. P. D. Sawaya, S. Sim, L. Veis, and A. Aspuru-Guzik, (2018), 1812.09976v2.

[7] A. W. Harrow, A. Hassidim, and S. Lloyd, *Physical Review Letters* **103** (2009), 10.1103/PhysRevLett.103.150502, *phys. Rev. Lett.* vol. 15, no. 103, pp. 150502 (2009), 0811.3171v3.

[8] A. Gilyén, Y. Su, G. H. Low, and N. Wiebe, (2018), 1806.01838v1.

[9] C. Shao and H. Xiang, *Phys. Rev. A* **101**, 022322 (2020).

[10] X. Xu, J. Sun, S. Endo, Y. Li, S. C. Benjamin, and X. Yuan, (2019), 1909.03898v1.

[11] C. Bravo-Prieto, R. LaRose, M. Cerezo, Y. Subasi, L. Cincio, and P. J. Coles, (2019), 1909.05820v1.

[12] H.-Y. Huang, K. Bharti, and P. Rebentrost, (2019), 1909.07344v2.

[13] I. Kerenidis and A. Prakash, (2018), 1808.09266v1.

[14] I. Kerenidis and A. Prakash, (2017), 1704.04992v3.

[15] E. Farhi, J. Goldstone, and S. Gutmann, (2014), 1411.4028v1.

[16] A. M. Childs and J.-P. Liu, (2019), 1901.00961v1.

[17] J. J. García-Ripoll, (2019), 1909.06619v1.

[18] J. M. Arrazola, T. Kalajdzievski, C. Weedbrook, and S. Lloyd, (2018), 1809.02622v1.

[19] S. Srivastava and V. Sundararaghavan, (2018), 1812.10572v2.

[20] T. Xin, S. Wei, J. Cui, J. Xiao, I. Arrazola, L. Lamata, X. Kong, D. Lu, E. Solano, and G. Long, (2018), 1807.04553v1.

[21] D. W. Berry, A. M. Childs, A. Ostrander, and G. Wang, *Communications in Mathematical Physics* **356**, 1057 (2017), *communications in Mathematical Physics* 356, 1057-1081 (2017), 1701.03684v2.

[22] D. W. Berry, (2010), 10.1088/1751-8113/47/10/105301, *j. Phys. A: Math. Theor.* 47, 105301 (2014), 1010.2745v2.

[23] S. K. Leyton and T. J. Osborne, (2008), 0812.4423v1.

[24] K. Griffin, S. Jain, T. Flint, and W. Chan, .

[25] A. M. Childs, J.-P. Liu, and A. Ostrander, (2020), 2002.07868v1.

[26] B. N. Todorova and R. Steijl, *Journal of Computational Physics* **409**, 109347 (2020).

[27] M. Lubasch, J. Joo, P. Moinier, M. Kiffner, and D. Jaksch, (2019), 1907.09032v2.

[28] P. C. S. Costa, S. Jordan, and A. Ostrander, *Physical Review A* **99** (2019), 10.1103/PhysRevA.99.012323, *phys. Rev. A* 99, 012323 (2019), 1711.05394v1.

[29] A. Bamberger, G. Chavent, and P. Lailly, *Applied Mathematics & Optimization* **5**, 1 (1979).

[30] A. Bamberger, G. Chavent, and P. Lailly, *Ann. Geophys* **33**, 2 (1977).

[31] A. M. Childs, D. Maslov, Y. Nam, N. J. Ross, and Y. Su, *Proceedings of the National Academy of Sciences* **115**, 9456 (2018), *proceedings of the National Academy of Sciences* 115, 9456-9461 (2018), 1711.10980v1.

[32] D. W. Berry, A. M. Childs, and R. Kothari, in *2015 IEEE 56th Annual Symposium on Foundations of Computer Science* (2015) pp. 792–809, *proceedings of the 56th IEEE Symposium on Foundations of Computer Science (FOCS 2015)*, pp. 792-809 (2015), 1501.01715v3.

[33] G. R. Ahokas, *Improved Algorithms for Approximate Quantum Fourier Transforms and Sparse Hamiltonian Simulations*, mastersthesis, University of Calgary (2004).

[34] D. W. Berry, G. Ahokas, R. Cleve, and B. C. Sanders, *Communications in Mathematical Physics* **270**, 359 (2007), *communications in Mathematical Physics* 270, 359 (2007), quant-ph/0508139v2.

[35] P. J. Coles, S. Eidenbenz, S. Pakin, A. Adedoyin, J. Ambrosiano, P. Anisimov, W. Casper, G. Chennupati, C. Coffrin, H. Djidjev, D. Gunter, S. Karra, N. Lemons, S. Lin, A. Lokhov, A. Malyzhenkov, D. Mascarenas, S. Mniszewski, B. Nadiga, D. O’Malley, D. Oyen, L. Prasad, R. Roberts, P. Romero, N. Santhi, N. Simit-syn, P. Swart, M. Vuffray, J. Wendelberger, B. Yoon, R. Zamora, and W. Zhu, (2018), 1804.03719v1.

[36] G. H. Low and I. L. Chuang, *Physical Review Letters* **118** (2017), 10.1103/PhysRevLett.118.010501, *phys. Rev. Lett.* 118, 010501 (2017), 1606.02685v2.

[37] G. H. Low and I. L. Chuang, “Hamiltonian simulation by qubitization,” (2016), only available as eprint, no journal publication., 1610.06546v2.

[38] G. H. Low and I. L. Chuang, “Hamiltonian simulation by uniform spectral amplification,” (2017), only available as eprint. No journal publication., 1707.05391v1.

[39] G. H. Low, (2018), 1807.03967v1.

[40] D. W. Berry and A. M. Childs, *Quantum Info. Comput.* **12**, 29 (2012), *quantum Information and Computation* 12, 29 (2012), 0910.4157v4.

[41] D. W. Berry, A. M. Childs, R. Cleve, R. Kothari, and R. D. Somma, *Physical Review Letters* **114** (2015),

10.1103/PhysRevLett.114.090502, phys. Rev. Lett. 114, 090502 (2015), 1412.4687v1.

[42] M. Kieferova, A. Scherer, and D. Berry, “Simulating the dynamics of time-dependent hamiltonians with a truncated dyson series,” (2018), only eprint on arXiv., 1805.00582v1.

[43] D. Shmoys, D. W. Berry, A. M. Childs, R. Cleve, R. Kothari, and R. D. Somma, in *Proceedings of the 46th Annual ACM Symposium on Theory of Computing - STOC 14* (2014) pp. 283–292, proceedings of the 46th ACM Symposium on Theory of Computing (STOC 2014), pp. 283-292 (2014), 1312.1414v2.

[44] A. M. Childs and N. Wiebe, (2012), 10.26421/QIC12.11-12, quantum Information and Computation 12, 901-924 (2012), 1202.5822v1.

[45] A. M. Childs and R. Kothari, in *Theory of Quantum Computation, Communication, and Cryptography* (Springer Berlin Heidelberg, 2011) pp. 94–103, theory of Quantum Computation, Communication, and Cryptography (TQC 2010), Lecture Notes in Computer Science 6519, pp. 94-103 (2011), 1003.3683v2.

[46] “Hamiltonian simulation implementation in qiskit-aqua,” [https://github.com/Qiskit/qiskit-aqua/blob/master/qiskit/aqua/operators/weighted\\_pauli\\_operator.py#L837](https://github.com/Qiskit/qiskit-aqua/blob/master/qiskit/aqua/operators/weighted_pauli_operator.py#L837) (2019), accessed: 2020-03-27.

[47] “Quantum algorithms for the simulation of hamiltonian dynamics,” <https://github.com/njross/simcount> (2019), accessed: 2020-03-27.

[48] A. Scherer, B. Valiron, S.-C. Mau, S. Alexander, E. van den Berg, and T. E. Chapuran, Quantum Information Processing **16** (2017), 10.1007/s11128-016-1495-5, quantum Inf Process (2017) 16: 60, 1505.06552v2.

[49] “14-qubit backend: IBM Q team,” IBM Q 16 melbourne backend specifications v1.3.0.” (2019), (2019), retrieved from <https://quantum-computing.ibm.com>.

[50] “Melbourne hardware operation execution time,” [https://github.com/Qiskit/ibmq-device-information/blob/master/backends/melbourne/V1/version\\_log.md#gate-specification](https://github.com/Qiskit/ibmq-device-information/blob/master/backends/melbourne/V1/version_log.md#gate-specification) (2019), accessed: 2020-03-27.

[51] “Melbourne gate specification,” <https://github.com/Qiskit/ibmq-device-information/tree/master/backends/melbourne/V1#gate-specification> (2019), accessed: 2020-03-27.

[52] A. C. Vazquez, *Quantum Algorithm for Solving Tri-Diagonal Linear Systems of Equations*, mastersthesis, ETH Zürich (2018).

[53] M. Suzuki, Physics Letters A **146**, 319 (1990).

[54] M. Suzuki, Journal of Statistical Physics **43**, 883 (1986).

[55] H. Thapliyal and N. Ranganathan, (2017), 10.1145/2491682, j. Emerg. Technol. Comput. Syst. 9 (2013) 17:1-17:31, 1712.02630v1.

[56] S. A. Cuccaro, T. G. Draper, S. A. Kutin, and D. P. Moulton, (2004), quant-ph/0410184v1.

[57] T. G. Draper, (2000), quant-ph/0008033v1.

[58] A. Barenco, A. Ekert, K.-A. Suominen, and P. Törmä, (1996), 10.1103/PhysRevA.54.139, quant-ph/9601018v1.

[59] R. Cleve and J. Watrous, (2000), quant-ph/0006004v1.

[60] T. Häner, M. Roetteler, and K. M. Svore, (2016), quantum Information and Computation, Vol. 17, No. 7 & 8 (2017), 1611.07995v2.

[61] “Constructing large controlled nots,” <https://algassert.com/circuits/2015/06/05/Constructing-Large-Controlled-Not.html> (2015), accessed: 2020-03-27.

[62] “Ibmq backends information,” <https://github.com/Qiskit/ibmq-device-information> (2019), accessed: 2020-03-27.

[63] “gprof2dot main page,” <https://github.com/jrfonseca/gprof2dot> (2019), accessed: 2020-03-27.

[64] A. M. Childs, Y. Su, M. C. Tran, N. Wiebe, and S. Zhu, (2019), 1912.08854v1.

[65] Y. Nam, N. J. Ross, Y. Su, A. M. Childs, and D. Maslov, npj Quantum Information **4** (2018), 10.1038/s41534-018-0072-4.

## Appendix A: Product-formula implementation details

### 1. Hamiltonian simulation

Hamiltonian simulation is the problem of constructing a quantum circuit that will evolve a quantum state according to a Hamiltonian matrix, following the Schrödinger equation. In other words, Hamiltonian simulation algorithms generate a quantum circuit performing the unitary transformation  $U$  such that  $\|U - e^{-iHt}\| < \epsilon$ ,  $H$  being a given Hamiltonian matrix,  $t$  a time of evolution and  $\epsilon$  a precision with respect to  $\|\cdot\|$ , the spectral norm.

Several quantum algorithms have been developed in the last few years to solve the problem of  $s$ -sparse Hamiltonian simulation [32, 34, 36–45]. Among these algorithms we decided to implement the product-formula approach [33, 34], for the reasons presented in Section III A.

The product formula algorithm has three main steps: decompose, simulate, recompose. It works by first decomposing the  $s$ -sparse Hamiltonian matrix  $H$  that should be simulated as a sum of Hermitian matrices  $H_j$  that are considered easy to simulate

$$H = \sum_{j=0}^{m-1} H_j. \quad (\text{A1})$$

The second step is then to simulate each  $H_j$  separately, i.e. to create quantum circuits implementing  $e^{-iH_j t}$  for all the  $H_j$  in the decomposition in Equation (A1). The last step uses the simulations computed in step two to approximate  $e^{-iHt}$ .

The very first questions that should be answered before starting any implementation of the product-formula algorithm are “What is an easy to simulate matrix?” and “What kind of Hermitian matrices are easy to simulate?”.

### 2. Easy to simulate matrices

One of the most desirable properties for an “easy to simulate” matrix is the possibility to simulate it exactly, i.e. to construct a quantum circuit that will perfectly implement  $e^{-iHt}$ . This property becomes a requirement when one wants rigorous bounds on the error of the final

simulation. Another enviable property of these matrices is that they can be simulated with a low gate number and only a few calls to the matrix oracle.

**Definition 3** (Easy to simulate matrix). A Hermitian matrix  $H$  can be qualified as “easy to simulate” if there exist an algorithm that takes as input a time  $t$  and the matrix  $H$  and outputs a quantum circuit  $C(H)_t$  such that

1. The quantum circuit  $C(H)_t$  implements exactly the unitary transformation  $e^{-iHt}$ , i.e.

$$\|e^{-iHt} - C(H)_t\| = 0.$$

2. The algorithm only needs  $\mathcal{O}(1)$  calls to the oracle of  $H$  and  $\mathcal{O}(\log N)$  additional gates,  $N$  being the dimension of the matrix  $H$ .

With this definition of an “easy to simulate” matrix, we can now search for matrices or group of matrices that satisfy this definition.

#### a. Multiples of the identity

The first and easiest matrices that fulfil the easy to simulate matrix requirements are the multiples of the identity matrix  $\{\alpha I, \alpha \in \mathbb{R}\}$  with  $I$  the identity matrix. The quantum circuit to simulate this class of matrices can be found in [52].

#### b. 1-sparse Hermitian matrices

A larger class of matrices that can be efficiently and exactly simulated are the 1-sparse, integer weighted, Hermitian matrices. Quantum circuits simulating exactly 1-sparse matrices with integer weights can be found in [33].

**Note 5.** Procedures simulating 1-sparse matrices with real (non-integers) weights are also described in the paper, but these matrices do not fall in the “easy to simulate” category because the procedures explained are exact only if all the matrix weights can be represented exactly with a fixed-point representation, which is not always verified.

**Note 6.** Multiples of identity matrices presented in Section A 2 a are a special case of 1-sparse matrices. The two classes have been separated because more efficient quantum circuits exists for  $\alpha I$  matrices.

### 3. Decomposition of $H$

Once the set of “easy to simulate” matrices has been established, the next step of the algorithm is to decompose the  $s$ -sparse matrix  $H$  as a sum of matrices in this set.

There are two possible ways of performing this decomposition, each one with its advantages and drawbacks: applying a procedure computing the decomposition automatically, or decompose the matrix  $H$  beforehand and provide the decomposition to the algorithm.

The first solution, which is to automatically construct the oracles of the  $H_j$  matrices from the oracle of the  $H$  matrix has been studied in [33] and [45]. Thanks to this automatic decomposition procedure, we only need to implement one oracle. This simplicity comes at the cost of a higher gate count: each call to the automatically constructed oracles of the matrices  $H_j$  will require several calls to the oracle of  $H$  along with additional gates.

On the other hand, the second solution offers more control at the cost of less abstraction and more work. The decomposition of  $H$  is not automatically computed and should be performed beforehand. Once the matrix  $H$  has been decomposed as in Equation (9), the oracles for the matrices  $H_j$  should be implemented. This means that we should now implement  $m$  oracles instead of only 1 for the first solution. The main advantage of this method over the one using automatic-decomposition is that it gives us more control, a control that can be used to optimize even more the decomposition of Equation (A1) (less  $H_j$  in the decomposition,  $H_j$  matrices that can be simulated more efficiently, ...).

All the advantages and drawbacks weighted, we chose to implement the second option for several reasons. First, the implementation of the automatic decomposition procedure adds a non-negligible implementation complexity to the whole Hamiltonian simulation procedure. Moreover, the automatic decomposition procedure can be implemented afterwards and plugged effortlessly to the non-automatic implementation. Finally, our use-case only required to simulate a 2-sparse Hamiltonian that can be decomposed as the sum of two 1-sparse Hermitian matrices, which makes the manual decomposition step manageable.

### 4. Simulation of the $H_j$

Once the matrix  $H$  has been decomposed following Equation (A1) with each  $H_j$  being an “easy to simulate” matrix, the simulation of  $H_j$  becomes a straightforward application of the procedures described in Section A 2.

After this step, we have access to quantum circuits implementing  $e^{-iH_j t}$  for  $j \in [0, m - 1]$  and  $t \in \mathbb{R}$ .

### 5. Re-composition of the $e^{-iH_j t}$

The ultimate step of the algorithm is to approximate the desired evolution  $e^{-iHt}$  with the evolutions  $e^{-iH_j t}$ . In the special case of mutually commuting  $H_j$ , this step is trivial as it boils down to use the properties of the exponential function on matrices and write  $e^{iHt} = e^{i \sum_j H_j t} =$

$\prod_j e^{iH_j t}$ . But in the more realistic case where the matrices  $H_j$  do not commute, a more sophisticated method should be used to approximate the evolution  $e^{-iHt}$ . To this end, we used the first-order Lie-Trotter-Suzuki product formula defined in Definition 4.

**Definition 4** (Lie-Trotter-Suzuki product formula [31, 53, 54]). The Lie-Trotter-Suzuki product formula approximates

$$\exp \left( \lambda \sum_{j=0}^m \alpha_j H_j \right) \quad (\text{A2})$$

with

$$S_2(\lambda) = \prod_{j=0}^{m-1} e^{\alpha_j H_j \lambda/2} \prod_{j=m-1}^0 e^{\alpha_j H_j \lambda/2} \quad (\text{A3})$$

and can be generalized recursively to higher-orders

$$S_{2k}(\lambda) = [S_{2k-2}(p_k \lambda)]^2 \times S_{2k-1}((1-4p_k)\lambda) [S_{2k-2}(p_k \lambda)]^2 \quad (\text{A4})$$

with  $p_k = (4 - 4^{1/(2k-1)})^{-1}$  for  $k > 1$ . Using this formula, we have the approximation

$$e^{\lambda H} = \left[ S_{2k} \left( \frac{\lambda}{n} \right) \right]^n + \mathcal{O} \left( \frac{|\lambda|^{2k+1}}{n^{2k}} \right). \quad (\text{A5})$$

We used the Lie-Trotter-Suzuki product formula with  $\lambda = -it$  to approximate the operator  $e^{-iHt}$  up to an error of  $\epsilon \in \mathcal{O} \left( \frac{t^{2k+1}}{n^{2k}} \right)$ .

## Appendix B: Hermitian matrix construction and decomposition

One of the main challenge in implementing a quantum wave equation solver lies in the construction and implementation of the needed oracles. This appendix describes the first step of the implementation process: the construction and decomposition of the Hamiltonian matrix that will be simulated using the Hamiltonian simulation procedure introduced in Appendix A.

This appendix follows the analysis performed in [28] and adds details and observations that will be refereed to in Appendix C when dealing with the actual oracle implementation.

### 1. Hamiltonian matrix description

In order to devise the Hamiltonian matrix that should be simulated to solve the wave equation, the first step is to discretise Equation (1) with respect to space. Such a discretisation can be seen as a graph  $G_{\delta x}$  whose vertices are the discretisation points and with edges between

nearest neighbour vertices. The graph  $G_{\delta x}$  is depicted in Figure 8.

The graph Laplacian of  $G_{\delta x}$ , defined as

$$L(G_{\delta x})_{i,j} := \begin{cases} \deg(v_i) & \text{if } i = j \\ -1 & \text{if } (i \neq j) \wedge (v_i \text{ adjacent to } v_j) \\ 0 & \text{otherwise} \end{cases} \quad (\text{B1})$$

can then be used to approximate the differential operator  $\frac{\partial^2}{\partial x^2}$ . By using the discretisation approximation

$$\frac{\partial^2 \phi}{\partial x^2}(i\delta x, t) \approx \frac{\phi_{i-1,t} - 2\phi_{i,t} + \phi_{i+1,t}}{\delta x^2} \quad (\text{B2})$$

with  $\phi_{i,t} = \phi(i\delta x, t)$ , and approximating  $\phi(x, t)$  with a vector  $\phi = [\phi_{i,t}]_{0 \leq i < N_d}$ , the matrix

$$A = -\frac{1}{\delta x^2} L(G_{\delta x}) \quad (\text{B3})$$

approximates the second derivative of  $\phi$  when  $\delta x \rightarrow 0$  as

$$[A\phi]_i = \frac{\phi((i-1)\delta x, t) - 2\phi(i\delta x, t) + \phi((i+1)\delta x, t)}{\delta x^2}. \quad (\text{B4})$$

The approximation (B3) is then used in Equation (1) to approximate the spatial derivative operator:

$$\frac{\partial^2}{\partial t^2} \phi = -\frac{1}{\delta x^2} L(G_{\delta x}) \phi. \quad (\text{B5})$$

Based on this formula, [28] shows that simulating

$$H = \begin{pmatrix} 0 & B \\ B^\dagger & 0 \end{pmatrix} \quad (\text{B6})$$

with

$$BB^\dagger = L \quad (\text{B7})$$

constructs a quantum circuit that will evolve a part of the quantum state it is applied on according to the discretised wave equation (B5).

A matrix  $B$  satisfying (B7) can be obtained directly from the graph  $G_{\delta x}$  representing the discretisation. The algorithm to construct the matrix  $B$  can be decomposed in three steps. First, the vertices (discretisation points) should be arbitrarily ordered by assigning them a unique index in  $[0, N_d - 1]$ . Then, each edge of the graph is arbitrarily oriented and indexed with indices in  $[0, N_d - 2]$ . Finally,  $B$  is computed with the following definition

$$B_{ij} = \begin{cases} 1 & \text{if edge } j \text{ is a self-loop of vertex } i, \\ 1 & \text{if edge } j \text{ has vertex } i \text{ as source,} \\ -1 & \text{if edge } j \text{ has vertex } i \text{ as sink,} \\ 0 & \text{otherwise} \end{cases}. \quad (\text{B8})$$

Note that edges' orientation and vertices/edges ordering is completely arbitrary. Changing either the edges orientation on one of the orderings will change the matrix  $B$  but will not affect  $BB^\dagger$  which should be equal to  $L$ . This freedom in the ordering and orientation choices takes a crucial importance in the oracle implementation as it allows us to pick the ordering/orientation that will produce an easy-to-implement matrix  $B$ .



Figure 8. Graph  $G_{\delta x}$  built from the discretisation of the 1-dimensional line  $[0, 1]$  with  $N_d$  discretisation points (i.e.  $\delta x = \frac{1}{N_d-1}$ ).

## 2. Dirichlet boundary conditions

Fixing boundary conditions is a requirement for most of the partial differential equations to admit a unique well-defined solution. There exist several boundary conditions such as Neumann, Dirichlet, Robin or Cauchy ones. For simplicity, we restricted ourselves to the study of Equation (1) with Dirichlet boundary condition of Equation (2).

In the case of Dirichlet boundary conditions on the 1-dimensional line  $[0, 1]$ , the two boundary nodes at  $x = 0$  and  $x = 1$  can be ignored as their value is always equal to 0. Moreover, [28] shows that the graph  $G_{\delta x}^D$  representing the discretisation with Dirichlet boundary conditions (2) is simply  $G_{\delta x}$  with self-loops on the two outer nodes (i.e. the ones indexed 1 and  $N_d-2$  as 0 and  $N_d-1$  are ignored).  $G_{\delta x}^D$  is depicted in Figure 9.

## 3. Matrices construction

All the pieces are now in place to start building the matrix  $B_d \in \mathbb{R}^{(N_c-1) \times N_c}$ . Using the definition of the matrix  $B$  written in Equation (B8) and the graph  $G_{\delta x}^D$  depicted in Figure 9 we end up with

$$B_d = \begin{pmatrix} 1 & 1 & 0 & \cdots & 0 \\ 0 & -1 & 1 & \ddots & \vdots \\ \vdots & \ddots & \ddots & \ddots & 0 \\ 0 & \cdots & 0 & -1 & 1 \end{pmatrix} \quad (\text{B9})$$

We can easily check that  $B_d B_d^\dagger$  is equal to the well-known discretisation matrix

$$B_d B_d^\dagger = \begin{pmatrix} 2 & -1 & 0 & \cdots & 0 \\ -1 & 2 & \ddots & \ddots & \vdots \\ 0 & \ddots & \ddots & \ddots & 0 \\ \vdots & \ddots & \ddots & 2 & -1 \\ 0 & \cdots & 0 & -1 & 2 \end{pmatrix}, \quad (\text{B10})$$

which validate the method of construction of  $B_d$ .

Computing  $\widetilde{H}_d$ , the Hamiltonian matrix that should be simulated to evolve the quantum state according to the wave equation (1) with Dirichlet boundary conditions, is now straightforward. Using Equation (B6), we directly obtain

$$\widetilde{H}_d = \frac{1}{\delta x} \begin{pmatrix} 0 & \cdots & \cdots & 0 & 1 & 1 & 0 & \cdots & 0 \\ \vdots & & & \vdots & 0 & -1 & 1 & \ddots & \vdots \\ \vdots & & & \vdots & \ddots & \ddots & \ddots & \ddots & 0 \\ 0 & \cdots & \cdots & 0 & 0 & \cdots & 0 & -1 & 1 \\ 1 & 0 & \cdots & 0 & 0 & \cdots & \cdots & \cdots & 0 \\ 1 & -1 & \ddots & \vdots & \vdots & & & & \vdots \\ 0 & 1 & \ddots & 0 & \vdots & & & & \vdots \\ \vdots & \ddots & \ddots & -1 & \vdots & & & & \vdots \\ 0 & \cdots & 0 & 1 & 0 & \cdots & \cdots & \cdots & 0 \end{pmatrix} \quad (\text{B11})$$

As explained in Appendix A, the Hamiltonian simulation algorithm implemented requires that the Hamiltonian to simulate is split as a sum of 1-sparse Hermitian matrices. There are a lot of valid decompositions for the matrix  $\widetilde{H}_d$  and we are free to choose the decomposition that will simplify the most the oracle implementation or reduce the gate complexity.

We made the choice to decompose  $B_d$  as two 1-sparse matrices and then reflect this decomposition on  $\widetilde{H}_d$ . Let  $B_1$  and  $B_{-1}$  defined as

$$B_1 = \begin{pmatrix} 0 & 1 & 0 & \cdots & 0 \\ \vdots & \ddots & 1 & \ddots & \vdots \\ \vdots & & \ddots & \ddots & 0 \\ 0 & \cdots & \cdots & 0 & 1 \end{pmatrix} \quad (\text{B12})$$

$$B_{-1} = \begin{pmatrix} 1 & 0 & \cdots & \cdots & 0 \\ 0 & -1 & \ddots & & \vdots \\ \vdots & \ddots & \ddots & \ddots & \vdots \\ 0 & \cdots & 0 & -1 & 0 \end{pmatrix} \quad (\text{B13})$$

we have  $B_d = B_1 + B_{-1}$ . Let also

$$\widetilde{H}_1 = \frac{1}{\delta x} \begin{pmatrix} 0 & B_1 \\ B_1^\dagger & 0 \end{pmatrix}, \quad \widetilde{H}_{-1} = \frac{1}{\delta x} \begin{pmatrix} 0 & B_{-1} \\ B_{-1}^\dagger & 0 \end{pmatrix}, \quad (\text{B14})$$

it is easy to see that  $\widetilde{H}_d = \widetilde{H}_1 + \widetilde{H}_{-1}$  and that both  $\widetilde{H}_1$  and  $\widetilde{H}_{-1}$  are 1-sparse Hermitian matrices.

For convenience, we also define

$$H_1 = \begin{pmatrix} 0 & B_1 \\ B_1^\dagger & 0 \end{pmatrix}, \quad H_{-1} = \begin{pmatrix} 0 & B_{-1} \\ B_{-1}^\dagger & 0 \end{pmatrix}, \quad (\text{B15})$$

and  $H_d = H_1 + H_{-1}$ , the  $\widetilde{H}_1$ ,  $\widetilde{H}_{-1}$  and  $\widetilde{H}_d$  matrices rescaled to contain only integer weights. These matrices

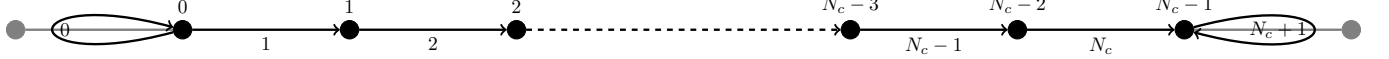


Figure 9. Graph  $G_{\delta x}^D$  representing the discretisation of the 1-dimensional line  $[0, 1]$  with Dirichlet boundary conditions. The points and edges in grey are only drawn for illustration purpose and are ignored in the analysis because the boundary condition impose a value of 0 on these vertices. Loops are added to  $G_{\delta x}$  to encode the fact that this graph represents Dirichlet boundary conditions. Vertices (resp. edges) are ordered with indices within  $[0, N_c - 1]$  (resp.  $[0, N_c + 1]$ ).  $N_c$  is the number of considered points and is equal to  $N_d - 2$  (the two extremal points are ignored).

have the interesting property that simulating  $\widetilde{H}_d$  (resp.  $\widetilde{H}_1, \widetilde{H}_{-1}$ ) for a time  $t$  is equivalent to simulating  $H_d$  (resp.  $H_1, H_{-1}$ ) for a time  $\frac{t}{\delta x}$ . This property will be used in the following sections as it offers us the opportunity to simulate the integer-weighted matrices  $H_d, H_1$  and  $H_{-1}$  instead of the real-weighted ones  $\widetilde{H}_d, \widetilde{H}_1$  and  $\widetilde{H}_{-1}$ .

Note also that a lower bound of the number of qubits needed to solve the wave equation for  $N_d$  discretisation points can be computed from the dimensions of  $H_d$ . As the non-empty upper-left block of matrix  $H_d$  is of dimension  $(2N_d - 1) \times (2N_d - 1)$ , we need at least

$$\lceil \log_2(2N_d - 1) \rceil \quad (\text{B16})$$

qubits to simulate it. This estimation does not take into account ancilla qubits that may be needed to implement the oracles.

### Appendix C: Oracle construction

Oracles can be seen as the interface between a quantum procedure and real-world data. Their purpose is to encode classical data such that a quantum algorithm can process it efficiently.

#### 1. Oracle interface

In order to work as a bridge between the classical and the quantum worlds and to be used by the quantum algorithm, a clear interface for the oracle should be established.

We chose to use the interface described in [33, Eq. 4.4] with slight modifications improving the arity of the oracle for our specific case of 1-sparse matrices.

More precisely, our oracles  $O$  implement the following interface

$$O |x_0\rangle |0\rangle |0\rangle |0\rangle = |x_0\rangle |m(x_0)\rangle |v(x_0)\rangle |s(x_0)\rangle \quad (\text{C1})$$

with  $|x_0\rangle$  encoding a row index as a unsigned integer,  $m(x)$  the function that returns the column index of the only non-zero element in row  $x$ ,  $v(x) = |w(x)|$  the absolute value of the weight  $w(x)$  of the first non-zero element in row  $x$  and

$$s(x) = \begin{cases} 0 & \text{if } w(x) \geq 0 \\ 1 & \text{else} \end{cases}. \quad (\text{C2})$$

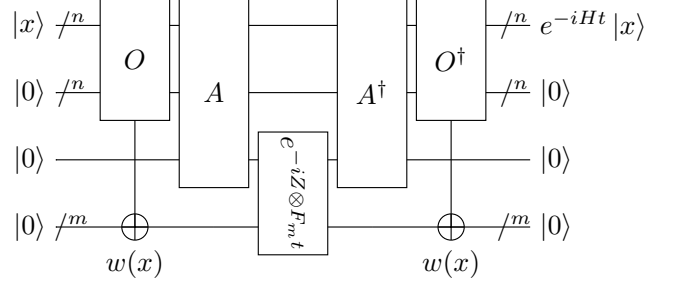


Figure 10. Quantum circuit re-created from [33, p. 71] that simulates a 1-sparse integer-weighted Hamiltonian for a given time  $t$ .  $F_m$  is defined as the diagonal matrix with diagonal entries increasing from 0 to  $2^m - 1$ .

the sign of the first non-zero entry in row  $x$ .

The interface of the oracle  $O$  can also be obtained with 3 separate oracles that will each take care of computing one output:

$$M |x_0\rangle |0\rangle = |x_0\rangle |m(x)\rangle \quad (\text{C3})$$

$$V |x_0\rangle |0\rangle = |x_0\rangle |v(x)\rangle \quad (\text{C4})$$

$$S |x_0\rangle |0\rangle = |x_0\rangle |s(x)\rangle \quad (\text{C5})$$

#### 2. Optimisation of $M$ and $S$

**Claim 1.** *The simulation algorithms provided by [33] have the interesting property that if the oracle  $V$  encodes a weight of zero for some inputs (i.e.  $v(x) = 0$  for some  $x$ ) then the outputs of oracles  $M$  and  $S$  are ignored for those inputs.*

*Proof.* The circuit simulating a 1-sparse  $m$ -bit-integer weighted Hamiltonian  $H$  depicted in Figure 10 is taken from [33].

In our special case of 1-bit weights (i.e.  $m = 1$ ), the

third quantum gate  $e^{-iZ \otimes Ft}$  can be written as

$$\begin{aligned} e^{-iZ \otimes Ft} &= \exp \left[ -i \begin{pmatrix} F & 0 \\ 0 & -F \end{pmatrix} t \right] \\ &= \begin{pmatrix} e^{-iFt} & 0 \\ 0 & e^{iFt} \end{pmatrix} \\ &= \begin{pmatrix} 1 & 0 & 0 & 0 \\ 0 & e^{-it} & 0 & 0 \\ 0 & 0 & 1 & 0 \\ 0 & 0 & 0 & e^{-it} \end{pmatrix}. \end{aligned} \quad (\text{C6})$$

where  $F = F_1$  and

$$F_m = \begin{pmatrix} 0 & 0 & \cdots & \cdots & \cdots & \cdots & 0 \\ 0 & 1 & \ddots & & & & \vdots \\ \vdots & \ddots & 2 & \ddots & & & \vdots \\ \vdots & & \ddots & 3 & \ddots & & \vdots \\ \vdots & & & \ddots & 4 & \ddots & \vdots \\ \vdots & & & & \ddots & \ddots & 0 \\ 0 & \cdots & \cdots & \cdots & \cdots & 0 & 2^m - 1 \end{pmatrix}. \quad (\text{C7})$$

It follows from the matrix notation that if the second qubit  $e^{-iZ \otimes Ft}$  is applied on is in the state  $|0\rangle$ , the gate  $e^{-iZ \otimes Ft}$  is the identity transformation, i.e. the unitary operation  $e^{-iZ \otimes Ft}$  sends  $|00\rangle$  (resp.  $|10\rangle$ ) to  $|00\rangle$  (resp.  $|10\rangle$ ). This means that if the oracle  $O$  does not set the last qubit to  $|1\rangle$  (i.e. encodes a weight of 0 for the  $x^{\text{th}}$  row of  $H$ ), the quantum circuit depicted in Figure 10 can be simplified up to an identity transformation as the effects of  $O$  (resp.  $A$ ) are reverted by  $O^\dagger$  (resp.  $A^\dagger$ ).

Rephrasing, if the  $x^{\text{th}}$  row of matrix  $H$  has no non-zero entries, the effects of the oracle  $O$  is ignored, which implies that the effects of the oracles  $M$  and  $S$  that compose  $O$  are also ignored.  $\square$

Using the result of Claim 1, we are free to implement any transformation that best suits us for the set of inputs  $|x\rangle$  such that the  $x^{\text{th}}$  row of the considered Hermitian matrix ( $H_1$  or  $H_{-1}$ ) has no non-zero elements as long as the oracle  $V$  implements the right transformation.

To illustrate clearly the *implemented* transformations we chose to encode with  $M$  and  $S$ , the next sections will re-write the matrices  $H_1$  and  $H_{-1}$  according to Equation (B15) but with one **0** or **-0** in each empty row. A **0** entry at position  $(i, j)$  in the matrix means that the row  $i$  was empty, the oracle  $M$  will map  $|i\rangle$  to  $|j\rangle$  and the oracle  $S$  will encode a positive sign, i.e.  $|0\rangle$ . The same reasoning applies for **-0** entries, except that the encoded sign is now negative, i.e.  $|1\rangle$ .

The following sections will explain step by step the construction of each of the three oracles  $M$ ,  $V$  and  $S$ , both for the matrix  $H_1$  ( $M_1$ ,  $V_1$  and  $S_1$ ) and the matrix  $H_{-1}$  ( $M_{-1}$ ,  $V_{-1}$  and  $S_{-1}$ ).

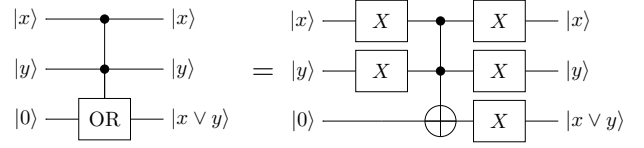


Figure 11. Implementation of the **or** gate.

### 3. About arithmetic and logic quantum gates

Implementing the oracles  $M$ ,  $V$  and  $S$  for the matrices  $H_1$  and  $H_{-1}$  requires several arithmetic and logic quantum gates such as **or**, **add** or **compare**.

All these gates have been implemented prior to the oracle implementation and the implementation steps are detailed in this section.

#### a. The **or** gate

The **or** gate is easily implemented using only **X** and **CCX** (or Toffoli) gates. The implementation used is depicted in Figure 11 and uses the famous Boolean algebra formula linking **not**, **or** and **and**:  $x \vee y = \neg(\neg x \wedge \neg y)$ .

#### b. The **add** and **sub** gates

Most of the research papers presenting an implementation of the **add** or **sub** gates only consider the case where the two numbers to add or subtract are stored in quantum registers.

In our case, the oracles implementation requires an adder and subtractor that can add or subtract to a quantum register a quantity known when the quantum circuit is generated, i.e. not necessarily encoded on a quantum state.

**Claim 2.** *Implementing a subtractor is trivial once an adder procedure is available.*

*Proof.* A subtractor can be implemented from a generic adder by using the identity

$$a - b = (a' + b)' \quad (\text{C8})$$

where ' denotes the bitwise complementation.

The circuit resulting of the application of this identity is depicted in Figure 12 and only requires one call to the adder and  $2n$  additional gates,  $n$  being the number of qubits used to represent one of the operands.  $\square$

**Note 7.** Following Claim 2 we will restrict the study to implementing an adder. Implementing a subtractor is trivial and cheap in term of additional quantum gates used once an adder is available.

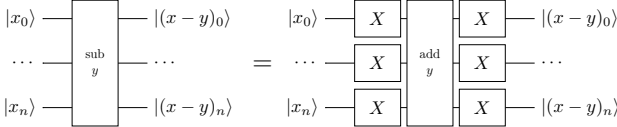


Figure 12. Implementation of the **sub** gate from an **add** gate. The  $y$  value encoding is intentionally omitted. The subtractor will use the same encoding as the adder (i.e. either the  $y$  value is encoded on a quantum register or it is encoded directly in the quantum circuit implementing the adder). Note that the  $y$  value is not negated.

**Definition 5.** *Generation-time value* A generation-time value is a value that is known by the programmer when generating the quantum circuit. Knowing a value at generation-time may allow to optimise even further the generated quantum circuit. The closest analog in classical programming would be C-like macros.

The easiest solution to overcome the problem caused by the non-compatible input formats is to encode the quantity known at generation-time into ancillary qubits and then use the regular adder algorithms to add to a quantum register the value encoded in a second quantum register. Even if this solution is trivial to implement, it has the huge downside of requiring  $\mathcal{O}(\log n)$  additional ancillary qubits to temporarily store the generation-time value.

Another answer to the problem would be to adapt a quantum adder originally devised to add two quantum registers to a quantum adder capable of adding a constant value to a quantum register. Several adders [55–57] have been studied to check if they can be modified to allow a generation-time input, i.e. if it possible to remove completely the quantum register storing the right-hand-side (or left-hand-side) of the addition.

The task of removing the quantum register storing one of the operands appears to be challenging for adders based on classical arithmetic like [55, 56] but trivial for Draper’s quantum adder introduced in [57].

**Claim 3.** *Draper’s quantum adder can be adapted into an efficient adder that takes as right-hand side input a unsigned “generation-time” integer value and add this value to a sufficiently large quantum register encoding another unsigned integer.*

*Proof.* The original Drapper’s adder as introduced in [57] is illustrated in Figure 13.

The only quantum gates using the quantum register  $|b\rangle$  are the controlled-phase gates. Moreover, they only use the qubits of the right-hand-side register  $|b\rangle$  as controls.

In the case of a constant value of  $b$  known at generation time, we can replace each controlled-phase gate by either a phase gate if the corresponding bit of  $b$  is 1 or by an identity gate (or a “no-op” gate) if the bit of  $b$  is 0. Once this transformation has been performed, the quantum register  $|b\rangle$  is no longer used and can be safely removed from the circuit.  $\square$

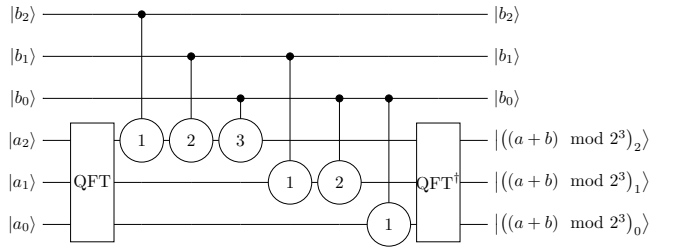


Figure 13. Original Draper’s adder example for 3-qubit registers  $|a\rangle$  and  $|b\rangle$ . The round gates between the two applications of the Quantum Fourier Transform (QFT gates) are controlled phase gates and are defined in [57]. Note that the adder wraps on overflow, meaning that if an overflow happens, the result will be  $(a + b) \bmod 2^3$ .

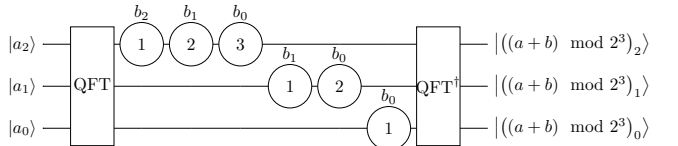


Figure 14. Modified Draper’s adder example for 3-qubit register  $|a\rangle$  and 3-bit classical constant  $b$ . The round gates between the two applications of the Quantum Fourier Transform (QFT gates) are phase gates and are defined in [57]. A label  $b_i$  above a phase gate means that the phase gate should only be applied when the  $i^{\text{th}}$  bit of  $b$  is set to 1. Note that the adder wraps on overflow, meaning that if an overflow happens, the result will be  $(a + b) \bmod 2^3$ .

The final quantum **add** gate implementation is depicted in Figure 14, requires  $\mathcal{O}(n^2)$  gates and has a depth of  $\mathcal{O}(n)$ . Following [57–59], the asymptotic gate count can be improved to  $\mathcal{O}(n \log(n))$  by removing the rotation with an angle below a given threshold that depend on hardware noise.

### c. The **cmp** gate

For the same reasons exposed in the adder implementation in Section C3b, the **cmp** gate cannot be implemented using the arithmetic comparator presented in [56] because removing the right-hand side qubits seems to be a challenging task.

Instead, we use the idea from [56, Section 4.3] that explain how to implement a comparator only by using a quantum adder. The comparison algorithm works by computing the high-bit of the expression  $a - b$ . If this high-bit is in the state  $|1\rangle$  then  $a < b$ .

In order to compute the high-bit of  $a - b$ , several options are open. The two most promising options are described in the following paragraphs.

The first option is to use a subtractor acting on  $n + 1$  qubits and behaving nicely on underflows (i.e. underflows result in cycling to the highest-value), as illustrated in Figure 15. This approach requires 2 calls to the subtrac-

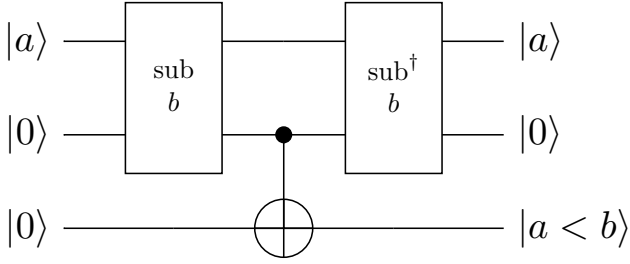


Figure 15. Computation of the high-bit of  $a - b$  with a  $n + 1$ -qubit subtractor. The second quantum register is an ancilla qubit that is appended to the quantum register storing  $|a\rangle$  in order to form a  $n + 1$ -qubit register. The result is stored in a third quantum register as  $|1\rangle$  if  $a < b$ , else  $|0\rangle$ .

tor and 1 additional 2-qubit quantum gate.

Another solution would be to use Equation (C8) to change the subtraction into an addition and then use a specialised procedure to compute the high-bit of the addition of two numbers  $a$  and  $b$  ( $a$  being encoded on a quantum register and  $b$  a constant). Computing the high-bit of an addition between a quantum register and a constant can be performed with the **CARRY** gate introduced in [60]. This approach requires  $\mathcal{O}(n)$  Toffoli, CNOT and X gates.

Each of the described methods has its advantages and drawbacks.

For example, the first method crucially relies on a quantum subtractor, and will have the same properties as the subtractor used. In our specific case, we use the subtractor implemented with Drapper’s adder [57] as explained in Section C 3 b, which in turn uses the quantum Fourier transform. The main disadvantage of using the QFT when looking at practical implementation on quantum hardware is that the QFT involves phase gates with exponentially small angles. These gates may be implemented correctly up to a given threshold, but very small rotation angles will inevitably not be as precise as *normal* rotation angles due to the hardware limitations in precision. This problem can be circumvented by using an approximate QFT algorithm [58, 59] that will cut all the rotation gates that have a rotation angle smaller than a given threshold from the generated circuit but the algorithm will not be exact anymore (small probability of incorrect result).

On the other hand, the **CARRY** gate involves only X, controlled-X and Toffoli gates. This restriction makes this implementation more robust than the first one to hardware errors or approximations and allows to simulate efficiently this gate on classical hardware as it only involves classical arithmetic.

As a last word, in the future, the QFT may be implemented directly into the hardware chips to make it more efficient because it is one of the most used quantum procedure (and so one of the best candidate for optimisation). Taking this possibility into account seems a little premature right now but may have a high impact on the

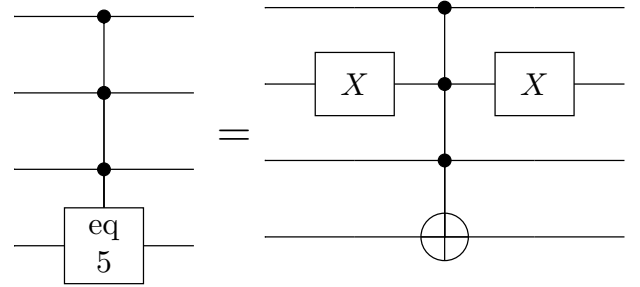


Figure 16. The **eq** gate implementation. X gates are applied to the second control qubit because the only bit set to 0 in the big-endian binary representation of  $5 = 101_2$  is at the second (middle) position.

efficiency and precision of the first solution presented.

After summarising all the drawbacks and advantages, we decided to use the arithmetic comparator for its linear number of gates, because it is based on arithmetic which does not involve exponentially small rotation angles and because the need to have  $n - 1$  dirty qubits to lend to the procedure is not an issue in our implementation.

#### d. The **eq** gate

The last gate the oracle implementation will need is an **eq** gate, testing the equality between an integer stored in a quantum register and a generation-time constant integer.

This gate has been implemented with a multi-controlled Toffoli gate and a few X gates before and after the control qubits of the Toffoli gates that should be equal to  $|0\rangle$ . The X gates are necessary because a raw Toffoli gate set its target qubit only when all its control are in the state  $|1\rangle$ , but we want each control qubit to be equal to a specific bit of the generation-time constant integer, which can be either  $|0\rangle$  or  $|1\rangle$ .

An implementation example is available in Figure 16.

Implementing a NOT gate controlled by  $n$  qubits can be done with only one ancilla qubit or  $n - 2$  garbage qubits and requires  $\mathcal{O}(n)$  X, controlled-X or Toffoli gates [61].

## 4. Oracles for $H_1$

As noted in Section C 2, the oracles  $M_1$  and  $S_1$  can be optimized by using the fact that they can encode anything for  $|x\rangle$  when the  $x^{\text{th}}$  row of  $H_1$  is empty.

We decided to use this optimization opportunity to add regularity to the description of the  $H_1$  matrix. The *implemented* matrix  $H_1$ , denoted as  $H_1^{\text{impl}}$ , is described in Equation (C9).

**Note 8.** All indices start at 0. The first row of a matrix has the index 0, the second row the index 1 and so on.

This convention is used to match Python's indexing that

starts at 0.

$$H_1^{\text{impl}} = \begin{pmatrix} & \overbrace{\hspace{1cm}}^{N_c} & \overbrace{\hspace{1cm}}^{N_c+1} & \overbrace{\hspace{1cm}}^{2^q-(2N_c+1)} \\ \left\{ \begin{array}{c} N_c \\ N_c+1 \\ 2^q - (2N_c+1) \end{array} \right\} & \begin{pmatrix} 0 & \cdots & \cdots & 0 & 0 & 1 & 0 & \cdots & 0 & 0 & \cdots & \cdots & \cdots & 0 \\ \vdots & & & \vdots & \vdots & \ddots & \ddots & \ddots & \vdots & \vdots & & & \vdots & \vdots \\ \vdots & & & \vdots & \vdots & \ddots & \ddots & \ddots & 0 & \vdots & & & \vdots & \vdots \\ 0 & \cdots & \cdots & 0 & 0 & \cdots & \cdots & 0 & 1 & 0 & & & \vdots & \vdots \\ 0 & \cdots & \cdots & 0 & 0 & \cdots & \cdots & \cdots & 0 & \mathbf{0} & & & \vdots & \vdots \\ 1 & \ddots & & \vdots & \vdots & & & & \vdots & 0 & & & \vdots & \vdots \\ 0 & \ddots & \ddots & \vdots & \vdots & & & & \vdots & \vdots & & & \vdots & \vdots \\ \vdots & \ddots & \ddots & 0 & \vdots & & & & \vdots & \vdots & & & \vdots & \vdots \\ 0 & \cdots & 0 & 1 & 0 & \cdots & \cdots & \cdots & 0 & 0 & \cdots & \cdots & \cdots & 0 \\ 0 & \cdots & \cdots & 0 & \mathbf{0} & 0 & \cdots & \cdots & 0 & 0 & \cdots & \cdots & \cdots & 0 \\ \vdots & & & \ddots & \mathbf{0} & \ddots & & & \vdots & \vdots & & & \vdots & \vdots \\ \vdots & & & & \ddots & \ddots & \ddots & & \vdots & \vdots & & & \vdots & \vdots \\ \vdots & & & & & \ddots & \mathbf{0} & 0 & 0 & & & & & \vdots & \vdots \\ \vdots & & & & & & \ddots & \mathbf{0} & 0 & & & & & \vdots & \vdots \\ 0 & \cdots & \cdots & \cdots & \cdots & \cdots & \cdots & 0 & \mathbf{0} & 0 & 0 & \cdots & \cdots & \cdots & 0 \end{pmatrix} & (C9) \end{pmatrix}$$

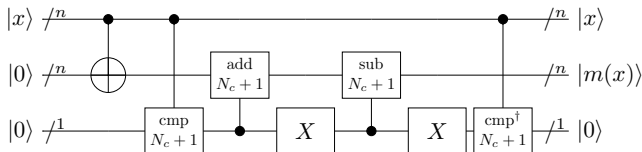


Figure 17. Implementation of the oracle  $M_1$ . The **cmp** gate compare the value of the control quantum register (interpreted as a unsigned integer) with the parameter given (written below the **cmp**). If the control register is strictly lower than the parameter, the gate set the qubit it is applied on to  $|1\rangle$ . The **add** (resp. **sub**) gate used in this quantum circuit add (resp. subtract) the value of its parameter to (resp. from) the quantum register it is applied on only if the control qubit is in the state  $|1\rangle$ .

According to the shape of the matrix in Equation (C9), the oracle  $M_1$  should implement the transformation

$$M_1|x\rangle|0\rangle \mapsto \begin{cases} |x\rangle|x + (N_c + 1)\rangle & \text{if } x < (N_c + 1) \\ |x\rangle|x - (N_c + 1)\rangle & \text{else} \end{cases} . \quad (\text{C10})$$

$M_1$  can be easily implemented with the quantum circuit depicted in Figure 17.

The oracle  $V$  cannot be simplified using the results from Claim 1. It should implement the transformation written in Equation (C11).

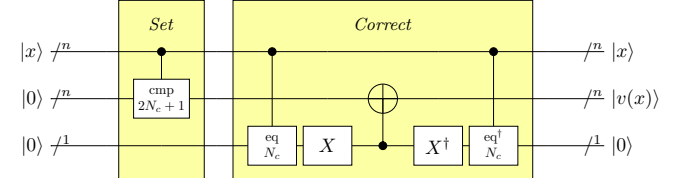


Figure 18. Implementation of the oracle  $V_1$ . The first part, *Set*, sets the qubit representing the weight to 1 for all  $|x\rangle$  such that  $x < 2N_c + 1$ . As this does not correspond to the correct expression of  $V$ , the second part *Correct* is here to set the weight register back to  $|0\rangle$  when  $|x\rangle = N_c$ . The **cmp** gate compare the value of the control quantum register (interpreted as a unsigned integer) with the parameter given (written below the **cmp**). If the control register is strictly lower than the parameter, the gate set the qubit it is applied on to  $|1\rangle$ . The **eq** gate used in this quantum circuit test if the value of its parameters equal to the quantum register it is applied on only if the control qubit is in the state  $|1\rangle$ .

$$V_1|x\rangle|0\rangle \mapsto \begin{cases} |x\rangle|1\rangle & \text{if } (x < 2N_c + 1) \wedge (x \neq N_c) \\ |x\rangle|0\rangle & \text{else} \end{cases} . \quad (\text{C11})$$

to simulate  $H_1$  is  $S_1$ , the oracle encoding the signs of the non-zero entries of  $H_1$ . The convention used to encode the sign of an entry has been taken from [33] and is: a positive sign is encoded as  $|0\rangle$ , a negative sign is encoded as  $|1\rangle$ . As shown in Equation (C9),  $H_1$  only contains positive non-zero entries so the sign oracle  $S_1$  should implement the simple transformation of Equation (C12): the identity.

$$S_1|x\rangle|0\rangle \mapsto |x\rangle|0\rangle \quad (C12)$$

### 5. Oracles for $H_{-1}$

The matrix  $H_{-1}$  has less regularity than  $H_1$ , which will lead to a more complex implementation. The *implemented* matrix  $H_{-1}$ , denoted as  $H_{-1}^{\text{impl}}$ , is described in Equation (C13).

$$H_{-1}^{\text{impl}} = \begin{pmatrix} & \overbrace{\quad}^{N_c} & \overbrace{\quad}^{N_c+1} & \overbrace{\quad}^{2^q - (2N_c+1)} \\ & 0 \dots \dots 0 & 1 0 \dots \dots 0 & 0 \dots \dots \dots 0 \\ & \vdots & 0 -1 \ddots & \vdots \\ & \vdots & \vdots \ddots \ddots \ddots & \vdots \\ & 0 \dots \dots 0 & 0 \dots 0 -1 0 & \vdots \\ & 1 0 \dots 0 & 0 \dots \dots \dots 0 & \vdots \\ & 0 -1 \ddots & \vdots & \vdots \\ & \vdots \ddots \ddots 0 & \vdots & \vdots \\ & \vdots \ddots -1 0 & \vdots & \vdots \\ & 0 \dots \dots 0 & -\mathbf{0} \ddots & 0 \dots \dots \dots 0 \\ & 0 \dots \dots 0 & -\mathbf{0} \ddots & 0 \dots \dots \dots 0 \\ & \vdots & \ddots \ddots \ddots & \vdots \\ & \vdots & \ddots 0 & \vdots \\ & \vdots & \ddots -\mathbf{0} 0 & \vdots \\ & 0 \dots \dots \dots \dots & \ddots -\mathbf{0} \ddots & \vdots \\ & 0 \dots \dots \dots \dots & 0 -\mathbf{0} 0 & \dots \dots 0 \end{pmatrix} \quad (C13)$$

Following the placement of the non-zero and the  $\mathbf{0}$  or  $-\mathbf{0}$  entries in the matrix  $H_{-1}^{\text{impl}}$  of Equation (C9), the oracle  $M_{-1}$  should implement the transformation

$$M_{-1}|x\rangle|0\rangle \mapsto \begin{cases} |x\rangle|x + N_c\rangle & \text{if } x < N_c \\ |x\rangle|x - N_c\rangle & \text{else} \end{cases} \quad (C14)$$

This transformation is quite similar to the one implemented by the oracle  $M_1$  in Equation (C10):  $N_c - 1$  from the transformation of  $M_1$  has been replaced by  $N_c$  in the transformation of  $M_{-1}$ . Thanks to this similarity, the implementation of  $M_{-1}$  will be a nearly-exact copy of the implementation of  $M_1$ . The full implementation of the  $M_{-1}$  oracle is depicted in Figure 19.

The weight oracle  $V_{-1}$  is the simplest to implement for the matrix  $H_{-1}$ , even if it cannot take advantage of the optimisation discussed in Claim 1. The transformation

that should be implemented by the oracle  $V_{-1}$  is shown in Equation (C15).

$$V_{-1}|x\rangle|0\rangle \mapsto \begin{cases} |x\rangle|1\rangle & \text{if } x < 2N_c \\ |x\rangle|0\rangle & \text{else} \end{cases} \quad (C15)$$

The implementation of the weight oracle  $V_{-1}$  is illustrated in Figure 20.

The last oracle left to implement is  $S_{-1}$ , the sign oracle. Due to the sign irregularity in the matrix  $H_{-1}^{\text{impl}}$ , the implementation of  $S_{-1}$  is more involved and requires several ancillary qubits. According to the shape of the matrix  $H_{-1}^{\text{impl}}$ , the sign oracle  $S_{-1}$  should implement the transformation defined in Equation (C16).

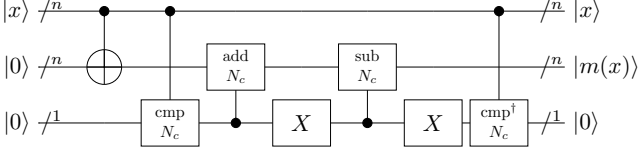


Figure 19. Implementation of the oracle  $M_{-1}$ . The **cmp** gate compare the value of the control quantum register (interpreted as a unsigned integer) with the parameter given (written below the **cmp**). If the control register is strictly lower than the parameter, the gate set the qubit it is applied on to  $|1\rangle$ . The **add** (resp. **sub**) gate used in this quantum circuit add (resp. subtract) the value of its parameter to (resp. from) the quantum register it is applied on only if the control qubit is in the state  $|1\rangle$ .

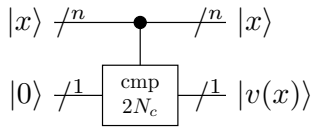


Figure 20. Implementation of the oracle  $V_{-1}$ . The **cmp** gate compare the value of the control quantum register (interpreted as a unsigned integer) with the parameter given (written below the **cmp**). If the control register is strictly lower than the parameter, the gate set the qubit it is applied on to  $|1\rangle$ .

$$S_{-1}|x\rangle|0\rangle \mapsto \begin{cases} |x\rangle|0\rangle & \text{if } (x = 0) \vee (x = N_c) \\ |x\rangle|1\rangle & \text{else} \end{cases}. \quad (\text{C16})$$

An implementation of the oracle  $S_{-1}$  is illustrated in Figure 21.

#### Appendix D: Note on precision

The Hamiltonian simulation algorithm we used to implement the wave equation solver still suffer from loose bounds on  $r$ , the number of time-step we should divide

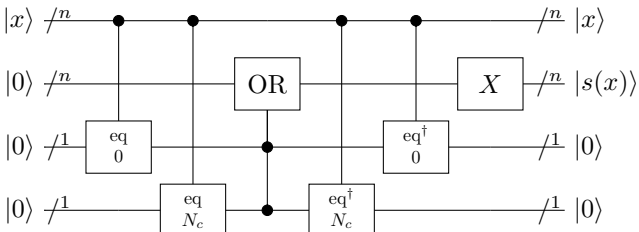


Figure 21. Implementation of the oracle  $S_{-1}$ . The **eq** gate used in this quantum circuit test if the value of its parameters equal to the quantum register it is applied on only if the control qubit is in the state  $|1\rangle$ . The **OR** gate flips the target qubit if and only if at least one of the two control qubits is in the state  $|1\rangle$ .

the evolution in in order to ensure that the error is at most  $\epsilon$ .

Several bounds exist to determine a  $r \in \mathbb{N}^*$  that will analytically ensure that the maximum allowable error  $\epsilon$  is not exceeded. The definition of such bounds can be found in [31, Appendix F] and is rewritten in the following equations.

The first bound has been devised by analytically bounding the error of simulation due to the Trotter-Suzuki formula approximation by  $\epsilon_0$

$$\left\| \exp \left( -it \sum_{j=0}^{m-1} H_j \right) - \left[ S_{2k} \left( -\frac{it}{r} \right) \right]^r \right\| \leq \epsilon_0 \quad (\text{D1})$$

and then let  $\epsilon_0 \leq \epsilon$  for a given desired precision  $\epsilon$ . If we let  $\Lambda = \max_j \|H_j\|$  and

$$\tau = 2m5^{k-1}\Lambda|t| \quad (\text{D2})$$

then

$$r_{2k}^{ana} = \left\lceil \max \left\{ \tau, \sqrt[2k]{\frac{e\tau^{2k+1}}{3\epsilon}} \right\} \right\rceil. \quad (\text{D3})$$

This bound is called the *analytic bound*.

A better bound called the *minimised bound* can be devised by searching for the smallest possible  $r$  that satisfies the conditions detailed in [31, Propositions F.3 and F.4]. This bound is rewritten in Equation (D4).

$$r_{2k}^{min} = \min \left\{ r \in \mathbb{N}^* : \frac{\tau^{2k+1}}{3r^{2k}} \exp \left( \frac{\tau}{r} \right) < \epsilon \right\} \quad (\text{D4})$$

The main issue with the analytic and minimised bounds is their looseness: even if the minimised bound improves over the analytic bound, both bounds can be orders of magnitudes higher from the optimal bound for some Hamiltonian matrices  $H$ . The analytic and minimised bounds are compared to the *empirical bound*, i.e. the optimal value of  $r$ , in Figure 22 for the matrix  $H = H_0 + H_1$  as defined in Equation (B11). From this comparison we see that in our specific case of  $H = H_0 + H_1$ , the minimised bound is quite close to the ideal empirical bound, which means that the overall performance of the implementation will not be improved a lot by a more precise bound.

#### Appendix E: Optimisation of the implementations

Both the Hamiltonian simulation and the wave equation solver circuits have been presented unoptimised. In this appendix we study possible optimisations that may be used on the implemented circuits to improve either the depth of the circuit or the number of gates used.

**Note 9.** As the wave equation solver uses the Hamiltonian simulation routine underneath, all the optimisations performed on the later will affect the former.

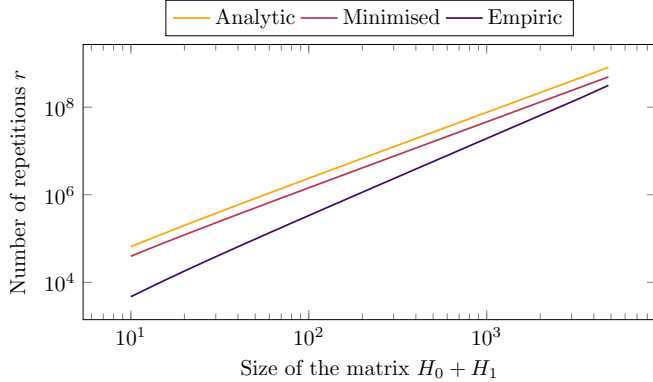


Figure 22. Plot of the repetition number  $r$  computed for the matrix  $H_0 + H_1$  with the analytic bound of Equation (D3), the minimised bound of Equation (D4) and the empirical bound which is the optimal value of  $r$ , computed by brute-force for small matrix sizes. This value of  $r$  has been computed for the product-formula introduced in Equation (A3) (i.e. the order  $k = 1$ ), a simulation time of  $t = 1$  and a target precision of  $\epsilon = 10^{-5}$ .

The methodology used to optimise a quantum program is the same as in classical computing:

1. Define the quantity we want to optimise. Most of the time, both in classical and quantum computing, the quantity of interest is the execution time. In the specific case of quantum computing, other quantities may be interesting to optimise, such as the number of S or T gates (for gate count optimisation when error correction codes are used) or the maximum idling time of each qubit (for coherence error minimisation).
2. Isolate the worst portions of code with respect to the quantity chosen in the first step. If we are interested in the total execution time, the best candidates for optimisation are the portions of code that take the most time to execute.
3. Improve the isolated portions of code with respect to the optimised quantity.
4. Return at step 2 until the overall code reach the target goal (for example “execution time divided by 2”) or the improvements made in the previous step are too small when compared to the effort delivered to optimise.

We followed this scheme to determine which subroutines are good candidates for optimisation. Because quantum program are ultimately bound to be run on quantum hardware, we chose to optimise the execution time on a real quantum chip. Only a few constructor give access to the characteristics of their chips and one of them is IBM. All the characteristics of IBM Q chips are available online on [62] and via Qiskit API. We chose to use IBM Q 16 Melbourne V1.3.0 because it is the largest

chip in terms of number of qubits that was publicly available at the time of writing.

Once the quantity to optimise has been clearly set, the next step is to determine the most interesting routines to optimise. In classical computing, a lot of tools exists to gather runtime informations and visualise this data. One of the most famous tool is probably `gprof` which is able to approximate the time spent in each function and create a call graph. Sadly, this kind of tool is still non-existent in the field of quantum computing. That is why we created a quantum equivalent of `gprof`, called `qprof`, that outputs exactly the same data as `gprof` but for a quantum program.

The text output of `qprof` is enough to isolate the subroutines to optimise first, but a visual representation can be obtained by combining `qprof` with a `gprof`-compatible visualisation tool such as `gprof2dot` [63]. The output of `qprof` for the Hamiltonian simulation procedure implemented can be found in Figure 23. The same graph can be obtained for the wave equation solver. As the only difference between the wave equation solver and the Hamiltonian simulation routine of Figure 23 is the time of evolution (and so the number of repetitions  $r$ ), the produced graphs are the same except for some routines where a negligible difference of 0.1% between the two call-graphs have been observed. For this reason, we omitted the output of `qprof` for the quantum wave equation solver.

### 1. Hamiltonian simulation procedure optimisation

Figure 23 represent the simplified call graph of the Hamiltonian simulation procedure. A lot of information can be extracted from this call graph:

1. The `trotter_suzuki_formula` procedure is called  $r_0 = 1463$  times. Dividing the number of repetitions by a factor of  $k$  would divide the number of gates and the execution time by the same factor  $k$ .
2. More than 85% of the total execution time is spent in the oracles.
3. More than 75% of the total execution time is spent in the `arithmetic_compare` procedure.
4. More than half of the total execution time is spent in the `high_bit_compute` procedure.

From these observations, several optimisation strategies can be devised. Some are discussed in the following sections.

#### a. Optimising the number of repetitions $r$

One of the major cost of the algorithm comes from the number of repetitions  $r$  we need to perform in order to

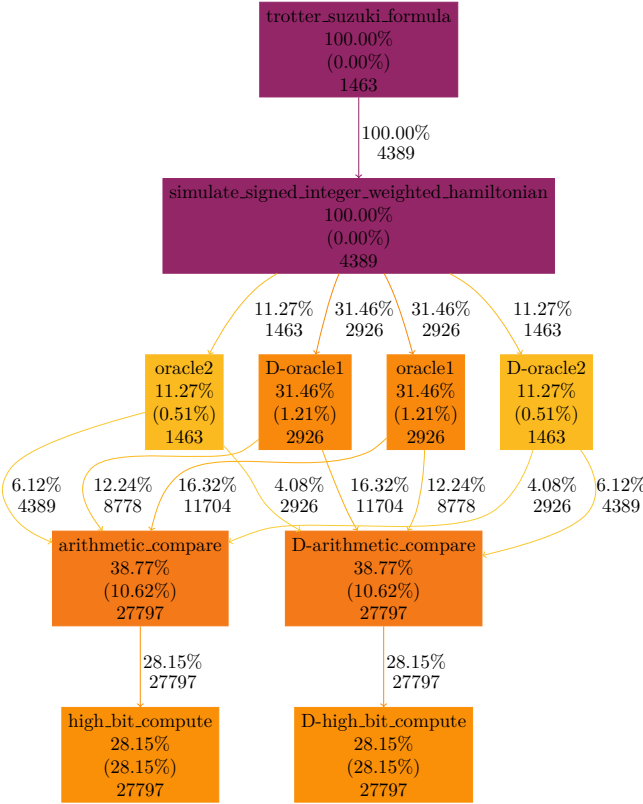


Figure 23. Reduced call-graph of the Hamiltonian Simulation routine implemented. Each node represent a quantum routine and contain the routine name, the total runtime of the routine (time spent in subroutines included), the self time of the routine (time spent only in the routine, not in subroutines) and the number of calls of the routine. A routine name starting with **D**- means that the routine has been inverted (**D**- is for dagger). All the nodes (i.e. sub-routines) taking less than 10% of the total time have been ignored. Instruction parallelism is not taken into account (the circuit is flattened before analysis).

ensure a given precision  $\epsilon$ . Several strategies can be used to try to reduce the number of repetitions  $r$ .

A first strategy could be to find a better upper-bound

for  $r$  than  $r_{2k}^{ana}$  (see Equation (D3)) and  $r_{2k}^{min}$  (see Equation (D4)). Such a bound can be found in [64]. This strategy could be interesting if the gap between the empiric and the minimised bounds was bigger in Figure 22. As the bound  $r_{2k}^{min}$  seems to tend towards  $r^{emp}$ , we believe that the potential gain of this optimisation will not be significant enough.

Another way of improving the number of repetitions  $r$  would be to use a more precise approximation, for example by using  $S_{2k}(\lambda)$  with  $k > 1$ . But using a higher-order approximation also increase the number of calls to the oracles by a factor  $5^k$ .

#### b. Optimising the subroutines

The call graph in Figure 23 allows us to isolate the procedures that contribute the most to the total execution time: **high\_bit\_compute** with more than 55% of the total runtime.

The choice we made in Section C 3 c to compare a quantum register and a constant classical value with a procedure computing the high-bit of a subtraction turns out to be a crucial step for the overall solver performances.

One idea of optimisation would be to use another algorithm to compare a quantum register with a constant value. The procedure using Drapper’s adder in Section C 3 c might be a good candidate on quantum hardware that can perform the QFT efficiently for example.

#### c. LCR optimisation

In parallel of all the other optimisation methods, automatic quantum circuit optimisers can be applied to all or parts of the quantum wave equation solver.

One of the most promising optimisation procedure for our wave equation solver is probably the LCR method used with an automatic circuit optimisation algorithm, both of which can be found in [65]. The LCR method is specifically designed to optimise quantum circuits that consist in the repetition of the same circuit a number  $N \geq 3$  times.